Magnetoresistance in polycrystalline and epitaxial $Fe_{1-x}Co_xSi$ thin films

N. A. Porter,[*] G. L. Creeth, and C. H. Marrows[†]
School of Physics and Astronomy, University of Leeds, Leeds LS2 9JT, United Kingdom
(Received 13 June 2012; revised manuscript received 19 July 2012; published 17 August 2012)

Thin films of $Fe_{1-x}Co_xSi$ were grown using molecular beam epitaxy on Si(111). These 20-nm-thick films, with compositions $x = 0$ or 0.5, were produced by two methods: the first produced large (111)-textured crystallites of the B20 phase; the second produced phase-pure B20 (111) epilayers. The lattice mismatch with the substrate causes biaxial tensile strain in the layers, greater in the epilayers, that distorts the (111)-oriented material to a rhombohedral form. Magnetotransport measurements show that a combination of additional scattering arising from crystal grain boundaries and strain-free polycrystalline films results in a higher resistivity than for the epitaxial films. Magnetometry for $x = 0.5$ suggests an increase in the ordering temperature in strained films relative to the polycrystalline films of 15 ± 4 K. Moreover, the characteristic linear magnetoresistance, typical of bulk single-crystal material of this composition, is retained in the polycrystalline film but reduced in the epitaxial film. While the bulk properties of these materials are reproduced qualitatively, there are small quantitative modifications, due to the strain, to properties such as band gap, Curie temperature, and magnetoresistance.

DOI: 10.1103/PhysRevB.86.064423 PACS number(s): 72.20.My, 68.55.−a, 73.50.Jt

I. INTRODUCTION

The transition-metal (TM) monosilicides are isostructural over the series from CrSi to NiSi.[1,2] Substitution of the TM can be used to tune a variety of low-temperature magnetic and electrical transport characteristics, the origins of which arise from the B20 crystal structure. At low temperatures FeSi has a paramagnetic, narrow-gap semiconductor ground state,[3,4] while TM substitution dramatically alters the magnetic phase of the material through doping. The addition of holes by substituting Mn for Fe produces a paramagnetic metal, whereas electron doping with Co can engineer a material with a helimagnetic metallic state[2] in addition to other more unconventional spin textures.[5] These are a result of the lack of inversion symmetry in the B20 structure. This property encourages neighboring moments to be canted by a small angle as a result of Dzyaloshinskii-Moriya interactions, resulting in helical patterns and skyrmion lattice textures which can give rise to a topological addition to the Hall effect.[6] A linear increase in conductivity upon electron doping is observed for $Fe_{1-x}Co_xSi$ for concentrations of Co in the range $0 < x < 0.4$. It has been shown that for every Co atom substituted for Fe in FeSi, one electron is added as a carrier while there is a corresponding contribution of one Bohr magneton to the magnetic moment.[2,7,8] This implies that for low Co concentration, $Fe_{1-x}Co_xSi$ could provide a 100% spin-polarized source of electrons.

In order to utilize the extraordinary properties reported in bulk materials in spintronic devices thin films are required, and attempts have been made to produce epitaxial thin films of $Fe_{1-x}Co_xSi$ with mixed success. Molecular beam epitaxy (MBE) has been used to produce films in a variety of available metastable phases.[9] Using Si(111) as a substrate, von Känel *et al*. produced the CsCl structure in addition to the stable (B20) bulk structure.[10] The CsCl structure has also been stabilized on Si(111) after production of polycrystalline FeSi by pulsed laser annealing,[11] a technique that has also been used to produce polycrystalline $Fe_{1-x}Co_xSi$.[12] More recently, solid-phase epitaxy has produced MnSi films on Si(111),[13] a technique used previously to produce FeSi on Si(100).[14] There are few reports on the effects of reduced dimensions on magnetotransport in these thin films, although magnetotransport on chemically grown $Fe_{1-x}Co_xSi$ nanowires has been reported.[15]

Here we report the growth of polycrystalline and epitaxial $Fe_{1-x}Co_xSi$ grown by MBE on Si(111), although we have become aware (after carrying out the current research) of a similar technique used to grow MnSi.[16] Although MnSi possesses the same B20 structure as $Fe_{1-x}Co_xSi$, it is a helimagnetic metal with a very different band structure and correspondingly different transport properties. The intrinsic strain of the TM monosilicide at the interface to Si(111) increases for the heavier TM elements as the lattice parameter is reduced. Because of the extreme sensitivity of the alloys' magnetism to crystal structure,[17] strain in the films can be expected to alter the transport properties significantly. We present magnetotransport and magnetometry data on both polycrystalline and epitaxial films influenced by both strain and disorder.

II. SAMPLE GROWTH AND CHARACTERIZATION

Thin films were prepared using MBE by coevaporation of Fe, Co, and Si onto Si(111) substrates from electron beam sources at a total rate of 0.3–0.6 Å s^{-1}. The growth chamber base pressure was 5×10^{-11} mbar. Wafers with a resistivity of 2000–3000 Ω cm at room temperature (used in order to minimize shunting through the substrate during electrical transport measurements) were prepared by flash annealing to 1200 °C *in situ* prior to evaporation. This produced the characteristic 7×7 reconstruction of the Si(111) surface, observed by low-energy electron diffraction (LEED; not shown), suggesting a clean and ordered surface.

Two methods were used to produce the films. In each case, a 5.4-Å buffer layer of Fe was evaporated at room temperature, followed by coevaporation of $Fe_{1-x}Co_xSi$. In the first method, the $Fe_{1-x}Co_xSi$ alloy was grown at room temperature. This growth produced (111) B1 $Fe_{1-x}Co_xSi$ (CsCl) texture normal to the surface as seen in x-ray diffraction (XRD). We observe a similar spectrum to Fig. 1 for $x = 0.5$ with a slightly lower

 ©2012 American Physical Society

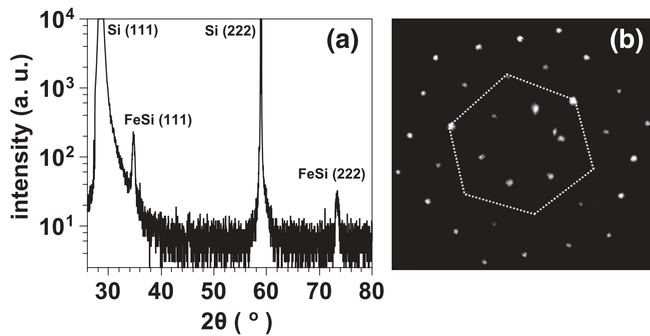

FIG. 1. (a) XRD of the 20-nm epitaxial film has narrow Bragg peaks corresponding to the B20 phase of FeSi. (b) LEED pattern taken at a beam energy of 100 eV of an identically grown FeSi surface after growth. The hexagon indicates the position of reciprocal lattice of the Si(111) substrate face based on LEED prior to growth. The FeSi diffraction pattern is rotated by 30° with respect to the Si surface reciprocal lattice.

intensity (111) Bragg peak from the film. Following the recipe of von Känel *et al.*,[10] *in situ* annealing at 400 °C for 1 h produced polycrystalline B20 $Fe_{1-x}Co_xSi$ apparent in the nonpreferentially orientated XRD spectra. From these spectra the Bragg reflections for the thin films are just visible above the measurement noise floor.

In the second method, the alloy was evaporated at 400 °C rather than room temperature. This produced an epitaxial (111) B20 phase confirmed by high-angle XRD, shown in Fig. 1(a), where, besides the Si substrate Bragg reflections, only the epitaxial Bragg peaks for the B20 structure are observed. This provided a lattice parameter of $d_{111} = 7.741 \pm 0.003$ Å. Figure 1(b) shows LEED of an FeSi film grown in identical conditions. The positions of the Si reciprocal surface unit cell measured prior to growth are also shown, illustrated by a dashed line.[18] The epitaxy is achieved by a 30° in-plane rotation of the $Fe_{1-x}Co_xSi$ unit cell relative to the Si substrate, aligning the $Fe_{1-x}Co_xSi$[110] parallel to the Si[112].[19] This produces a ∼6% biaxial in-plane tensile strain on the $Fe_{1-x}Co_xSi$ lattice. This deforms the cubic B20 structure to become slightly rhombohedral. XRD and LEED provide an overall profile of the epitaxial relationship between our film and the substrate.

For additional confirmation of the structure, cross-sectional high-resolution transmission electron micrographs (HRTEM) were taken to locally probe the ($x = 0$) Si-FeSi interface. Figure 2(a) illustrates a grain boundary of the polycrystalline film. The grains were ∼62 nm in lateral extent and extended vertically throughout the 20-nm height of the film. Figure 2(b) shows HRTEM of the epitaxial film. This illustrates matching of the FeSi(111) crystal with the Si(111) substrate. If the system were indeed cubic, then, provided with the out-of-plane lattice parameter d_{111}, from our XRD measurements the in-plane parameter d_{110} should be 6.3 ± 0.1 Å. HRTEM measurements show this to be larger, $d_{110} = 6.69 \pm 0.05$ Å, corresponding to the silicon substrate lattice parameter of $d_{112} = 6.7 \pm 0.1$ Å. These measurements confirm there is a 6% biaxial strain, as anticipated for epitaxial samples. The resulting unit cell is rhombohedral, with a characteristic angle of 92.5°. This is a slightly distorted cubic B20 structure. In

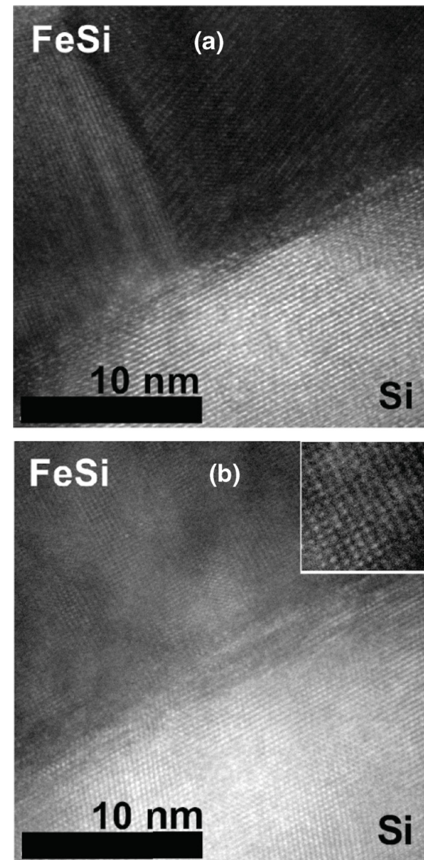

FIG. 2. HRTEM of (a) polycrystalline thin-film FeSi at the Si(111) interface and (b) epitaxial FeSi. A 3×3 nm^2 area of the FeSi epilayer is shown enlarged as an inset.

contrast to the polycrystalline film where ∼15 grain boundaries were observed per micron cross section, no grain boundaries were observed anywhere in the 4-μm-wide cross section of the epitaxial film.

III. MEASUREMENT METHODS

The thicknesses of all four films were measured using low-angle x-ray reflectometry, and all were within the range 20.5 to 20.9 nm. The samples were cleaved into approximately 2.5×9.0 mm^2 rectangles along the [110] edges of Si. The resistivity was measured using a standard in-plane four-probe dc technique, with the probes separated by 2.7 mm on the surface. The long axis defining the current direction for the epitaxial sample was along the $Fe_{1-x}Co_xSi$[112]. Measurements were performed in a He gas flow cryostat in applied magnetic fields up to 8 T. Vibrating sample magnetometry (VSM) was used to study the onset of magnetic ordering in the $x = 0.5$ films. For each measurement, in order to ensure a large signal-to-noise ratio, multiple fragments of the sample that were not used for transport measurements were stacked upon each other. Hysteresis loops were measured using an in-plane field. As multiple fractions of the original samples were used, it is likely that, for the epitaxial sample, some relative in-plane misalignment of the crystals would have arisen. Nevertheless, the applied magnetic field direction for the samples was close to the $Fe_{1-x}Co_xSi$[112] crystal orientation.

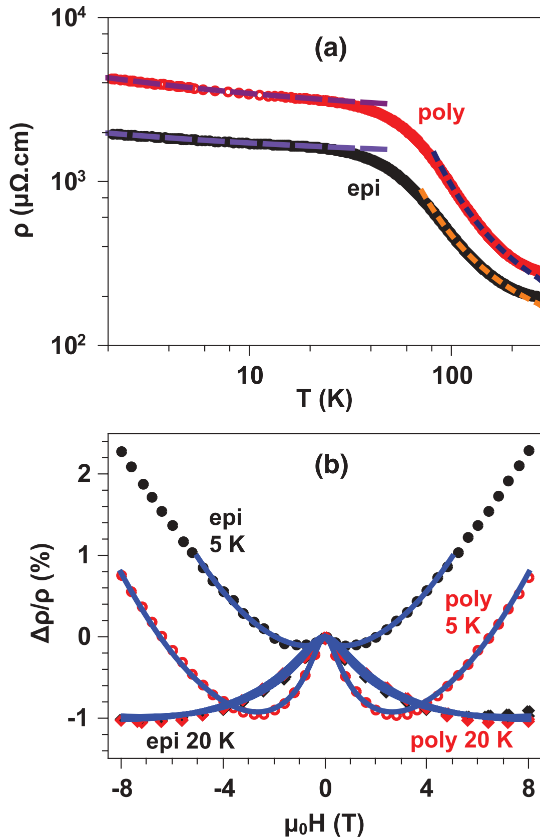

FIG. 3. (Color online) (a) Zero-field resistivity of parent compound FeSi 20-nm-thick films. Long-dashed fits illustrate the VRH regime, and short-dashed lines are fits to the data to estimate the energy gaps (see main text). (b) MR isotherms of each film at 5 K (circles) and 20 K (diamonds). At 20 K both films behave in a similar manner. At 5 K a larger negative component to the MR is observed in the polycrystalline film (open symbols) than in the epitaxially grown film (solid symbols). Fits (solid blue lines) correspond to WL suppression in a magnetic field in addition to a quadratic magnetic field dependence. (Only every eighth data point is shown.)

IV. MAGNETOTRANSPORT OF FeSi FILMS

Measurements of the parent structure, FeSi ($x = 0$), are shown in Fig. 3. Both films have a negative temperature coefficient of resistivity, as expected for this narrow energy gap semiconductor.[4,20] The resistivity ρ of the polycrystalline film exceeded that of the epitaxial film over the entire temperature T range. This is anticipated due to the additional scattering of conduction carriers from boundaries between crystallites when compared to the epitaxial film. There are two regimes apparent in the transport which cross over at 30 K. Below 30 K the conduction is mediated by three-dimensional (3D) variable range hopping (VRH),[20–22] as illustrated by the fits below 30 K for both curves obeying $\ln[\rho(B)/\rho(0)] \propto T^{-1/4}$. Above 30 K carriers thermally activated across the semiconducting energy gap Δ provide the main contribution to conduction. By assuming that the change in carrier density, rather than mobility, dominates the change in resistivity for each film the gap energy was estimated using $\ln\rho \propto \Delta/2k_BT$, fitted to data from Fig. 3(a), where k_B is Boltzmann's constant. From this assumption the gap energies of epitaxial and polycrystalline films were $\Delta_{EPI} = 26.9 \pm 0.1$ meV and $\Delta_{POLY} = 35.5 \pm 0.1$ meV, respectively, values similar to those measured in bulk material.[23–26]

Biaxial strain on the epitaxial FeSi relative to the assumed strain-free polycrystalline film may contribute to the differences in resistivity, by increasing the volume of the unit cell. Accounting for the 6% biaxial strain using the measured lattice parameters from HRTEM and XRD, it is possible to ascertain the volume V of both the epitaxial film ($V_{EPI} = 102 \pm 3$ Å^3) and the polycrystalline film ($V_{POLY} = 89.9 \pm 0.6$ Å^3). These parameters allow us to quantify the influence of the strain on the energy gap to be $d\ln\Delta/d\ln V = \ln(\Delta_{EPI}/\Delta_{POLY})/\ln(V_{EPI}/V_{POLY}) = -2.2 \pm 0.7$. This analysis suggests that strain on the crystal may influence the band structure by reducing the energy gap. Although only biaxial strain is considered here, as opposed to hydrostatic pressure in the literature, this value is similar to that of theory[27] (-5.9) and experimental trends, which suggest that pressure increases the band separation.[28–30] Biaxial in-plane strain (or, alternatively, uniaxial out-of-plane stress) as we show here for a cubic system with the (111) axis out of the plane would result in a rhombohedral crystal structure.[31] This anisotropic deformation might partially compensate for the change in volume and account for the smaller change in energy gap calculated here. These results suggest that with suitable substrates or piezoelectric materials one may be able to engineer the film properties with strain.

The magnetoresistance (MR), defined as $\Delta\rho/\rho = [\rho(H) - \rho(0)]/\rho(0)$, where H is the applied magnetic field, of the films at 20 and 5 K is shown in Fig. 3(b). At 20 K FeSi films exhibited negative MR, in keeping with bulk measurements, where contributions from both negative and positive MR have been reported.[4,32,33] Nearly identical trends were observed in both films at this temperature, reminiscent of an external magnetic field destroying coherent scattering that leads to weak localization (WL).

At 5 K both films possess a positive component to the MR that appears quadratic in field. This can be modeled by MR that occurs from the constriction of VRH site wave functions due to a transverse field.[21] This MR is predicted to obey $\ln[\rho(B)/\rho(0)] \propto B^m$ with $m = 2$ in the predominantly "weak" fields used here. A combination of both these influences, 2D WL[34] and the VRH field dependence, are used to fit the conductivity:

$$\sigma = \sigma(0)\exp(-aB^2) + \frac{e^2}{h\pi}\left[\Psi\left(\frac{1}{2} + \frac{B_2}{B}\right) - \Psi\left(\frac{1}{2} + \frac{B_1}{B}\right) - \ln\left(\frac{B_2}{B_1}\right)\right], \quad (1)$$

where Ψ is the digamma function. Fits of Eq. (1) to the data are shown in Fig. 3(b). The first term on the right-hand side of Eq. (1) arises from VRH using the scaling parameter a, which depends upon the hopping-site density and wave-function decay length of these sites.[21] The remaining two fitting parameters relate to the second term in the sum and are attributed to WL. This model assumes negligible influence from spin-orbit effects and magnetic impurity scattering, such that B_1 and B_2 are the characteristic fields for elastic and inelastic scattering, respectively.[35]

TABLE I. Thouless lengths extracted from fits to Eq. (1) for the FeSi 20-nm thin films.

λ_{Th} (nm)	5 K	20 K
Polycrystalline	32 ± 3	21 ± 2
Epitaxial	57 ± 7	23 ± 4

At 5 K the weak limit of VRH is only obeyed for magnetic fields less than 5 T, and fitting is limited to this field range. Although we cannot calculate the field for the weak-strong limit crossover directly, it may be that the magnetic length ($\sqrt{\hbar/eB}$) at 5 T, $\lambda = 11$ nm, no longer satisfies the necessary condition that it is much greater than the radius of the hopping wave function.[21] The length scale for phase-coherent scattering is known as the Thouless length[36] ($\lambda_{Th} = \sqrt{\hbar/4eB_1}$). At 20 K the Thouless length extracted from the fits of both epitaxial and polycrystalline films is ~22 nm (see Table I). This length is likely to be limited by inelastic scattering from thermally activated phonons. Both films will contain some intrinsic crystal defects and impurities, whether in the film of the epilayer or in the crystallites for the polycrystalline film. At 5 K this length scale for the polycrystalline sample is increased slightly to 32 ± 3 nm, implying an increase in the length scale for coherent scattering. For the epitaxial film the Thouless length increases much further to 57 ± 7 nm. At these low temperatures defects play a greater role as phonons are frozen out. In the polycrystalline film additional disorder, and hence scattering, introduced by grain boundaries restricts this value. In the epitaxial film, with significantly fewer grain boundaries, carriers travel much greater distances limited, in the main, by defects or impurities.

The contribution from scattering at grain boundaries is influential below 20 K. Above this temperature differences in the electron transport of the film should be intrinsic to the alloy itself rather than limited by this scattering. It is likely that the change in band structure (narrowing of the semiconducting energy gap) of the parent FeSi alloy is an effect of the strain imparted by the substrate, which increases the volume of the unit cell. We continue to see the impact of this strain upon the magnetic and magnetotransport properties of the electron-doped metallic alloy $Fe_{1-x}Co_xSi$, presented in the following two sections.

V. MAGNETOMETRY OF $Fe_{0.5}Co_{0.5}Si$ FILMS

Magnetometry of the polycrystalline sample below and above the ordering temperature at 5 and 80 K, respectively, is shown in Fig. 4(a). At 5 K there is a small, $\mu_0 H_c = 1.6 \pm 0.4$ mT, coercive field. In the epitaxial film [Fig. 4(b)], an opening of the hysteresis loop is observed; the increased coercive field is $\mu_0 H_c = 5.6 \pm 0.4$ mT. $M(H)$ loops taken above the ordering temperature of the films at 80 K are also shown in Figs. 4(a) and 4(b), neither of which has resolvable hysteresis. Hysteresis below the ordering temperature in the films is in contrast to bulk, where the material is a helimagnet with the propagation vector lying along one of the [100] cubic axes defined by weak anisotropic exchange[5,37,38] for which one would expect to see no hysteresis and hence no remnant magnetization. One origin of such remnant magnetization in

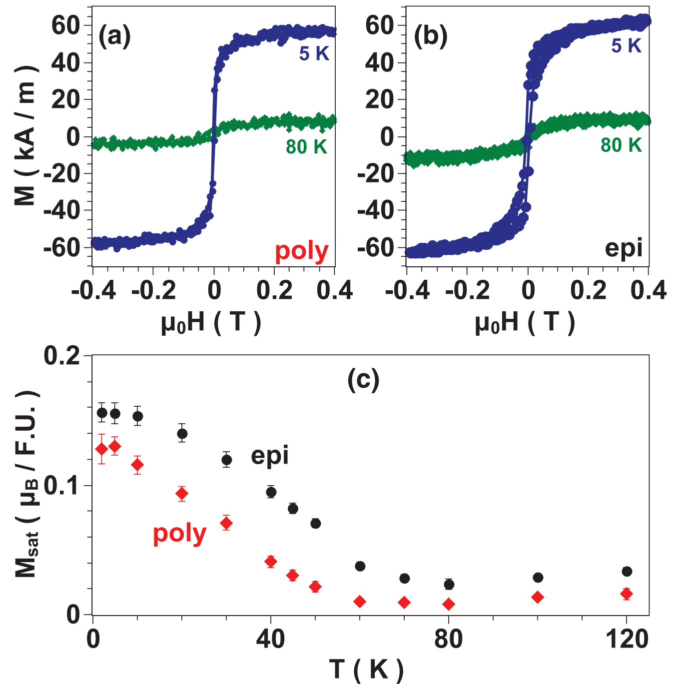

FIG. 4. (Color online) VSM of (a) polycrystalline and (b) epitaxial $Fe_{0.5}Co_{0.5}Si$ films with an in-plane magnetic field. (c) The saturation magnetization of both films as a function of temperature.

helical thin films is when uncompensated moments are retained in zero field when the film thickness is a noninteger multiple of the wavelength of the helix.[31]

Using isothermal hysteresis loops over the range 2–120 K the saturation magnetization was calculated using the unit-cell volume and the sample volume. These are shown in Fig. 4(c), where each data point was obtained from individual hysteresis loops. In $Fe_{1-x}Co_xSi$ for $0 < x < 0.25$ it is purported that the conduction electrons originating from the cobalt substitution possess one Bohr magneton, implying a fully-spin-polarized electron gas.[2] For higher electron doping, in our case, $x = 0.5$, this no longer holds true, and 0.15 μ_B per formula unit (f.u.) is anticipated.[2,7,30] Below 10 K the saturation magnetizations for the two samples are close to this bulk measured value, with a slightly higher saturation magnetization measured in the epitaxially grown films. By using the hysteresis loops, an Arrott plot method was used to ascertain the ordering temperatures T_c. In the polycrystalline film $T_c = 46 \pm 3$ K, in agreement with measured values for bulk.[2,5,30,38] For the epitaxial sample $T_c = 61 \pm 3$ K. This higher ordering temperature suggests that the magnetization may be stabilized by strain in the sample relative to the polycrystalline film. It is worth noting that in both films a slight increase in the saturation magnetization is observed as the samples are warmed beyond T_c. This arises from an increase in paramagnetic susceptibility occurring from thermally activated electrons excited into non-spin-split bands in a similar manner to that observed for $x = 0$ in FeSi.[3]

The magnetic characteristics of bulk $Fe_{0.7}Co_{0.3}Si$ have been measured by Onose *et al.*,[30] suggesting that the ordering temperature of this alloy is suppressed under hydrostatic pressure. These measurements imply a linear reduction of $dT_c/dP \sim -6.3$ K GPa^{-1} up to a pressure of 7 GPa,

above which the alloy becomes nonmagnetic. As there is a reduction in T_c under pressure for bulk, it is reasonable to anticipate the increase in T_c we observe for our strained films. For instance, the compressibility of the parent alloy FeSi is approximately linear,[39] $dP/dV \sim -2$ GPa Å^{-3}. If we expect a similar dT_c/dV and dT_c/dP for our $x = 0.5$ alloy, we predict $dT_c/dV = (dT_c/dP)(dP/dV) \sim 12.6$ K Å^{-3} for bulk hydrostatic compression. The 15 ± 4 K *increase* in ordering temperature we observe corresponds to an increase in the unit-cell volume from the polycrystalline film to the epitaxial film of ~12 Å^3, so that $\Delta T_c/\Delta V \sim 1.25$ K Å^{-3}. Hence we find the increase in T_c is smaller than we predict. Nevertheless, taking into account the assumptions used and the fact that films are under biaxial strain rather than hydrostatic pressure, we find an increase in ordering temperature for our films that is qualitatively in agreement with the experimental evidence on bulk $Fe_{1-x}Co_xSi$.

VI. MAGNETOTRANSPORT OF $Fe_{0.5}Co_{0.5}Si$ FILMS

Transport data for the doped films ($x = 0.5$) are shown in Fig. 5. Substitution of Co for Fe introduces carriers, producing a metallic temperature dependence of resistivity, as shown in Fig. 5(a). Again, the polycrystalline sample has a higher resistivity for the reasons outlined previously. The onset of linear MR below ~50 K coincides with the onset of magnetic ordering, as shown in Fig. 4. In Fig. 5(a) transport in an 8-T field is also included; below ~90 K a marked change in resistance is apparent in both films. MR isotherms are shown in Fig. 5(b).

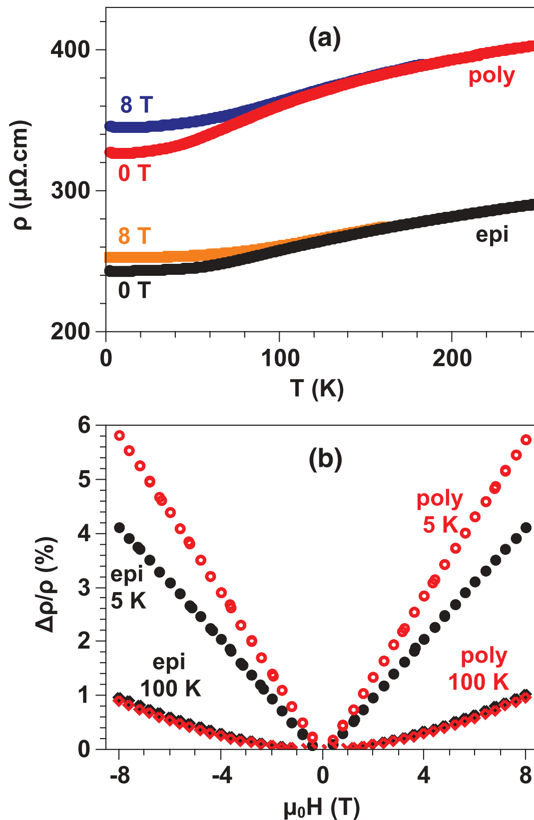

FIG. 5. (Color online) (a) Resistivity of doped $Fe_{1-x}Co_xSi$ 20-nm-thick films for $x \sim 0.5$ measured in 0 and 8 T magnetic fields. In each film a significant MR was noted below ~60 K. (b) MR isotherms of each film at 5 K (circles) and 100 K (diamonds). At 100 K both polycrystalline (open symbols) and epitaxial (solid symbols) films demonstrate similar quadratic MR. At 5 K a linear MR is observed in each film and is enhanced in the polycrystalline sample. (Only every eighth data point is shown.)

The MR at 100 K (above the Curie temperature) is shown in Fig. 5(b). This physical MR is quadratic in field, as anticipated for nonmagnetic carriers, arising from the Lorentz force acting on carriers with a momentum dispersion.[40] Importantly, it is almost identical in both films. At 5 K the MR is linear over the entire field range, which is characteristic of $Fe_{1-x}Co_xSi$,[2,15,30,41] although the origin is disputed.[2,30] Nevertheless, both descriptions emphasize the importance of a (nearly[30]) fully-spin-polarized electron gas to account for the observed MR, and there have been attempts to verify this experimentally.[42] The MR, which is dependent upon the B20 structure, is stronger in the polycrystalline film than the epitaxial film at 8 T, reaching almost 6% and 4%, respectively. The naive expectation might have been that that disorder from grain boundaries in the polycrystalline film would partially quench the effect; in fact, in the positive linear MR in epitaxial film the has a reduced magnitude. We note that a reduction in MR has been observed for bulk $Fe_{1-x}Co_xSi$ under hydrostatic pressure, in contrast to biaxial strain here.[43] The reduced MR in the epitaxial film relative to the polycrystalline film, along with the other physical properties discussed previously, may be attributed to strain in the epitaxial layer.

VII. CONCLUSION

In conclusion, both epitaxial and polycrystalline $Fe_{1-x}Co_xSi$ films have been produced on Si(111) using MBE. Epitaxial films registered with the substrate had a unit cell distorted from cubic to rhombohedral with a corresponding increase in unit-cell volume. This strain makes small quantitative modifications to almost all measured properties of both undoped and doped materials. For doped films we see an enhancement in the magnetic ordering temperature. Comparison of the electrical properties of $x = 0$ films suggests a reduction in the gap that may originate from the biaxial strain of the epitaxial film relative to the strain-free polycrystalline film. The influence of disorder from grain boundaries on the magnetotransport is evident from WL at low temperatures for the FeSi polycrystalline film. This disorder, also present in the doped samples ($x = 0.5$), does not appear to significantly suppress the linear MR below the magnetic ordering temperature whereas the MR in the strained epitaxial film is comparatively weaker. These modified electronic and magnetic properties are likely to affect the nature of chiral skyrmion states in these thin-film systems.

ACKNOWLEDGMENTS

The authors would like to acknowledge financial support from the UK EPSRC. We also thank Michael Ward for help with the TEM imaging and John Harrington for FIB sample preparation.

*n.a.porter@leeds.ac.uk
†c.h.marrows@leeds.ac.uk

[1] J. H. Wernick, G. K. Wertheim, and R. C. Sherwood, Mater. Res. Bull. **7**, 1431 (1972).
[2] N. Manyala, Y. Sidis, J. F. DiTusa, G. Aeppli, D. P. Young, and Z. Fisk, Nature (London) **404**, 581 (2000).
[3] V. Jaccarino, G. K. Wertheim, J. Wernick, L. Walker, and S. Arajs, Phys. Rev. **160**, 476 (1967).
[4] S. Paschen, E. Felder, M. A. Chernikov, L. Degiorgi, H. Schwer, H. R. Ott, D. P. Young, J. L. Sarrao, and Z. Fisk, Phys. Rev. B **56**, 12916 (1997).
[5] X. Z. Yu, Y. Onose, N. Kanazawa, J. H. Park, J. H. Han, Y. Matsui, N. Nagaosa, and Y. Tokura, Nature (London) **465**, 901 (2010).
[6] A. Neubauer, C. Pfleiderer, B. Binz, A. Rosch, R. Ritz, P. G. Niklowitz, and P. Böni, Phys. Rev. Lett. **102**, 186602 (2009).
[7] J. Guevara, V. Vildosola, J. Milano, and A. M. Llois, Phys. Rev. B **69**, 184422 (2004).
[8] S. A. Morley, N. A. Porter, and C. H. Marrows, Phys. Status Solidi RRL **5**, 429 (2011).
[9] A. I. Al-Sharif, M. Abu-Jafar, and A. Qteish, J. Phys. Condens. Matter **13**, 2807 (2001).
[10] H. von Känel, N. Onda, H. Sirringhaus, E. Müller-Gubler, S. Goncalves-Conto, and C. Schwarz, Appl. Surf. Sci. **70-71**, 559 (1993).
[11] C. M. Comrie, A. Falepin, O. Richard, H. Bender, and A. Vantomme, J. Appl. Phys. **95**, 2365 (2004).
[12] N. Manyala, B. D. Ngom, A. C. Beye, R. Bucher, M. Maaza, A. Strydom, A. Forbes, J. A. T. C. Johnson, and J. F. DiTusa, Appl. Phys. Lett. **94**, 232503 (2009).
[13] E. Karhu, S. Kahwaji, T. L. Monchesky, C. Parsons, M. D. Robertson, and C. Maunders, Phys. Rev. B **82**, 184417 (2010).
[14] J. Chrost, J. Hinarejos, P. Segovia, E. Michel, and R. Miranda, Surf. Sci. **371**, 297 (1997).
[15] A. L. Schmitt, J. M. Higgins, and S. Jin, Nano Lett. **8**, 810 (2008).
[16] E. A. Karhu, S. Kahwaji, M. D. Robertson, H. Fritzsche, B. J. Kirby, C. F. Majkrzak, and T. L. Monchesky, Phys. Rev. B **84**, 060404 (2011).
[17] M. P. J. Punkkinen, K. Kokko, M. Ropo, I. J. Väyrynen, L. Vitos, B. Johansson, and J. Kollar, Phys. Rev. B **73**, 024426 (2006).
[18] Le Tanh Vinh, J. Chevrier, and J. Derrien, Phys. Rev. B **46**, 15946 (1992).
[19] J. Chevrier, V. Le Thanh, S. Nitsche, and J. Derrien, Appl. Surf. Sci. **56–58**, 438 (1992).
[20] A. Mani, A. Bharathi, and Y. Hariharan, Phys. Rev. B **63**, 115103 (2001).
[21] B. I. Shklovskii and A. L. Efros, *Electronic Properties of Doped Semiconductors*, English ed., edited by S. Luryi, Solid State Sciences Vol. 45 (Springer, Berlin, 1984).
[22] P. Lunkenheimer, G. Knebel, R. Viana, and A. Loidl, Solid State Comm. **93**, 891 (1995).
[23] D. Zur, D. Menzel, I. Jursic, J. Schoenes, L. Patthey, M. Neef, K. Doll, and G. Zwicknagl, Phys. Rev. B **75**, 165103 (2007).
[24] T. Jarlborg, Phys. Rev. B **51**, 11106 (1995).
[25] C.-H. Park, Z.-X. Shen, A. G. Loeser, D. S. Dessau, D. G. Mandrus, A. Migliori, J. Sarrao, and Z. Fisk, Phys. Rev. B **52**, R16981 (1995).
[26] K. Breuer, S. Messerli, D. Purdie, M. Garnier, M. Hengsberger, Y. Baer, and M. Mihalik, Phys. Rev. B **56**, R7061 (1997).
[27] G. Grechnev, T. Jarlborg, A. Panfilov, M. Peter, and I. Svechkarev, Solid State Commun. **91**, 835 (1994).
[28] C. Reichl, G. Wiesinger, G. Zaussinger, E. Bauer, M. Galli, and F. Marabelli, Phys. B **259–261**, 866 (1999).
[29] A. Mani, Solid State Commun. **132**, 551 (2004).
[30] Y. Onose, N. Takeshita, C. Terakura, H. Takagi, and Y. Tokura, Phys. Rev. B **72**, 224431 (2005).
[31] E. A. Karhu, U. K. Rößler, A. N. Bogdanov, S. Kahwaji, B. J. Kirby, H. Fritzsche, M. D. Robertson, C. F. Majkrzak, and T. L. Monchesky, Phys. Rev. B **85**, 094429 (2012).
[32] H. Ohta, T. Arioka, Y. Yamamoto, S. Mitsudo, T. Hamamoto, M. Motokawa, Y. Yamaguchi, and E. Kulatov, Phys. B **237-238**, 463 (1997).
[33] V. Glushkov, I. Voskoboinikov, S. Demishev, I. Krivitskii, A. Menovsky, V. Moshchalkov, N. Samarin, and N. Sluchanko, J. Exp. Theor. Phys. **99**, 394 (2004).
[34] X. Wu, X. Li, Z. Song, C. Berger, and W. A. de Heer, Phys. Rev. Lett. **98**, 136801 (2007).
[35] Y. Wang and J. J. Santiago-Avilés, J. Appl. Phys. **94**, 1721 (2003).
[36] D. K. Ferry and S. M. Goodnick, *Transport in Nanostructures* (Cambridge University Press, Cambridge, 1997).
[37] M. Uchida, Y. Onose, Y. Matsui, and Y. Tokura, Science **311**, 359 (2006).
[38] S. V. Grigoriev, V. A. Dyadkin, D. Menzel, J. Schoenes, Y. O. Chetverikov, A. I. Okorokov, H. Eckerlebe, and S. V. Maleyev, Phys. Rev. B **76**, 224424 (2007).
[39] I. G. Wood, T. D. Chaplin, W. I. F. David, S. Hull, G. D. Price, and J. N. Street, J. Phys. Condens. Matter **7**, L475 (1995).
[40] A. B. Pippard, *Magnetoresistance in Metals* (Cambridge University Press, Cambridge, 1989).
[41] M. K. Chattopadhyay, S. B. Roy, S. Chaudhary, K. J. Singh, and A. K. Nigam, Phys. Rev. B **66**, 174421 (2002).
[42] J. P. DeGrave, A. L. Schmitt, R. S. Selinsky, J. M. Higgins, D. J. Keavney, and S. Jin, Nano Lett. **11**, 4431 (2011).
[43] M. K. Forthaus, G. R. Hearne, N. Manyala, O. Heyer, R. A. Brand, D. I. Khomskii, T. Lorenz, and M. M. Abd-Elmeguid, Phys. Rev. B **83**, 085101 (2011).